Appl. Magn. Reson. 6, 195–215 (1994)

Applied Magnetic Resonance

Very High Frequency EPR – 94 GHz Instrument and Applications to Primary Reaction Centers from Photosynthetic Red Bacteria and to Other Disordered Systems*

W. Wang[1], R.L. Belford[1], R.B. Clarkson[1], P.H. Davis[1,a], J. Forrer[1,b], M.J. Nilges[1], M.D. Timken[1,c], T. Walczak[1,d], M.C. Thurnauer[2], J.R. Norris[2,e], A.L. Morris[2,e], and Y. Zhang[2]

[1] Illinois EPR Research Center, Departments of Chemistry, Internal Medicine and Veterinary Clinical Medicine, University of Illinois at Urbana/Champaign, Urbana, Illinois, USA
[2] Chemistry Division, Argonne National Laboratory, Argonne, Illinois, USA

Received August 15, 1993

Abstract. There are many advantages to carrying out electron paramagnetic resonance experiments at very high frequencies, either as part of a multifrequency strategy for solving problems or for special characteristics of high frequencies. These special characteristics include the potential for high point sensitivity, enhanced resolution, separation of similar species, altered sensitivity to motion, suppression of motional effects, and many others. This paper describes a three-millimeter-wavelength (W-band, 94 GHz) EPR spectrometer built for a multi-user facility and illustrates with some examples, most of them being disordered systems. One significant example is the oxidized primary reaction center, P^{+}_{865}, isolated from the red photosynthetic bacteria *Rhodobacter Sphaeroides* R-26. The W-band technique applied to both centers isolated from bacteria grown from either deuterated or ordinary growth media allows extraction of the full g anisotropy in these centers and sets the stage for multifrequency EPR spectroscopy to yield a full analysis of the various contributions to linewidths in these systems.

1. Introduction

Most electron paramagnetic resonance (EPR, also known as ESR or EMR) experiments are performed at conventional 9 or 35 GHz frequencies. But in

* Adapted in substantial part from the PhD Dissertation of Wei Wang, University of Illinois, Urbana, April 1993.

[a] Current address: University of Tennessee at Martin, Martin, TN, USA
[b] Permanent address: ETH, Zürich, Switzerland
[c] Current address: Widener University, PA, USA
[d] Current address: Dartmouth Medical School, Hanover, NH 03755-3863, USA
[e] Also Department of Chemistry, University of Chicago, Chicago, IL 60637, USA

numerous situations, a large increase in the microwave frequency (and/or magnetic field) can result in substantial increase in the information content in EPR spectra [1]. This motivated us to construct a very high frequency (VHF) – 94 GHz – EPR spectrometer at the Illinois EPR Research Center (IERC). This paper describes some features of the spectrometer and illustrates some advantages of VHF EPR through application to selected disordered materials, including primary reaction centers isolated from photosynthetic red bacteria.

2. The W-band EPR Spectrometer

2.1. Overview of the W-band Spectrometer

Very few EPR spectrometers operate at very high (>60 GHz) microwave frequencies. Some are discussed in selective review articles and papers [2–13]. Most such spectrometers have been constructed by individual groups for specialized purposes. The VHF W-band (95 GHz) EPR spectrometer at IERC is designed as a versatile instrument for doing EPR spectroscopy in a multi-user facility. It is intended to accommodate a variety of chemical, biological, and material samples in a public accessible, multi-user facility. The first version of this spectrometer is described here; a version with enhanced capabilities is in development and will be described elsewhere.

The block diagram, Fig. 1, shows the basic layout of the W-band EPR spectrometer at IERC. Briefly, it is of the reflection-cavity-circulator type with a reference arm. The spectrometer uses a varactor-tuned solid-state diode source (ZAX, inc.) operating at 95 GHz with maximum output power >50 mW. A unique end-coupled frequency-tunable cylindrical TE_{013} or TE_{012} cavity has been designed and constructed to be specially robust, provide good mechanical stability and permitting the use of a field-replaceable iris. A Schottky diode operating at ambient temperature is currently serving as the microwave detector. The spectrometer uses a Varian NMR superconducting magnet, operating in persistent mode, and a locally-built air-cooled sweep coil, with 300 Gauss scan range. Alternatively, it uses an Oxford superconducting magnet with wide sweep capability (0–7 Tesla). The magnetic field can be monitored by a high precision NMR teslameter and the frequency is measured by an accurate counter. Phase-sensitive detection with 100 kHz field modulation has been used. Data acquisition is accomplished via A/D board in an IBM personal computer. All the major components can be computer-controlled through an IEEE-488 interface.

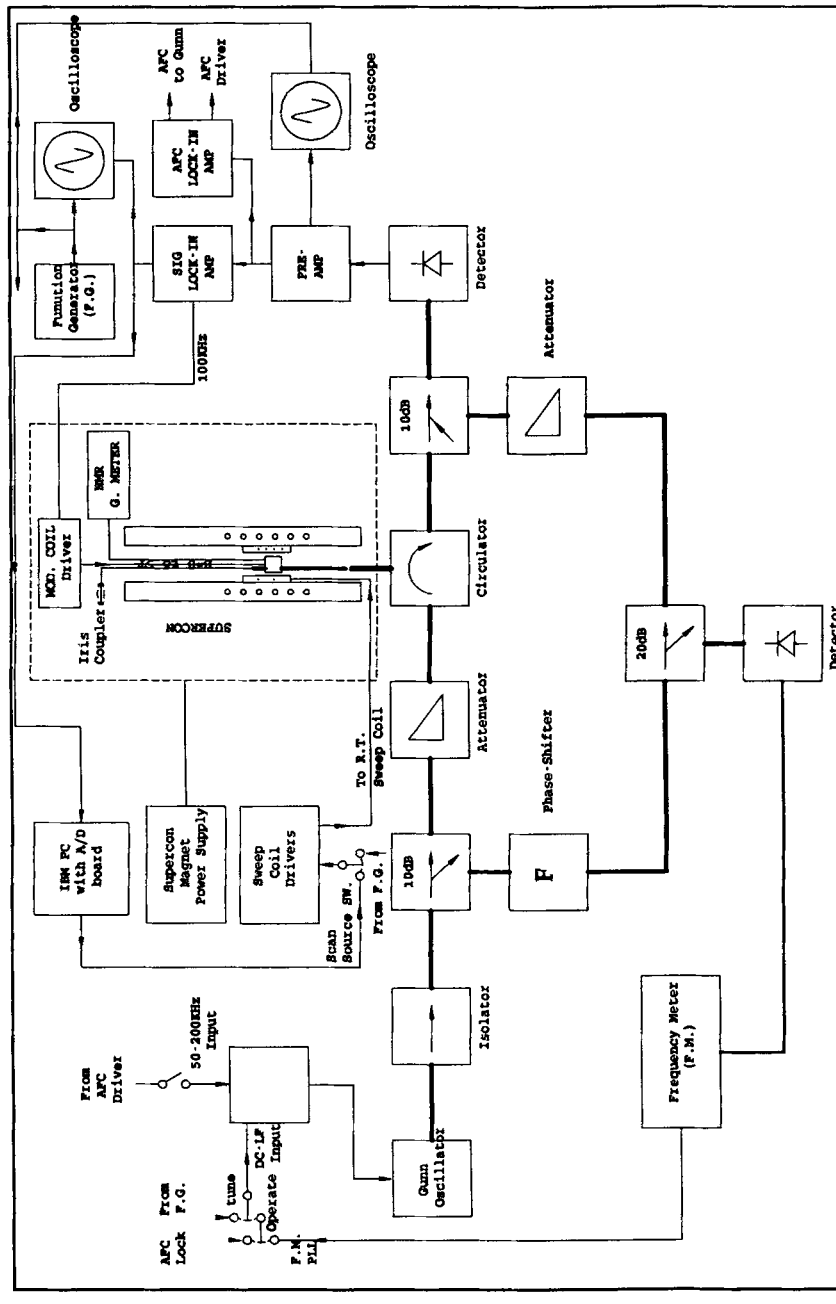

Fig. 1. Block diagram of the W-band EPR spectrometer system.

2.2. Details of the W-band Spectrometer

Microwave Source. Criteria for selecting a microwave source included noise performance, output power, tuning bandwidth, convenience, durability, and cost of replacement. Three different types of microwave sources have been tried: a Hughes varactor-tuned Gunn oscillator (Microwave Products Division, Torrance, CA), a klystron (Varian Canada, Georgetown, Ont.), and a ZAX varactor-tuned Gunn oscillator (ZAX Millimeter Wave Corporation, San Dimas, CA). The ZAX diode has the least phase noise and highest power output. For everyday routine measurement, a solid-state millimeter-wave Gunn oscillator is preferred for its relatively low cost, low-voltage supply requirements, and ruggedness. For applications requiring higher B_1 fields, a klystron can be used. The technical specifications of these three microwave sources are listed in Table 1. Solid-state sources have been quite inferior to klystrons in phase noise, but they have been improving in recent years. The noise performance of the Hughes Gunn oscillator employed earlier in the development of the spectrometer, the Varian klystron and the ZAX Gunn oscillator are compared in Fig. 2. Notice that the ZAX Gunn oscillator has FM noise that is comparable with that of the klystron, and considerably less than that of the older Hughes diode. For the many current applications involving only organic free radicals which are easily saturated at or above 1 mW, the power provided by a Gunn oscillator usually suffices and the ZAX Gunn oscillator becomes our choice for routine work.

Microwave Bridge. The microwave bridge is of a straightforward homodyne design. It consists of a main arm, a reference (bucking) arm, and a vertical arm. The reference arm provides an easy way to separate the absorption and dispersion signals and biases the detector diode into its high-sensitivity region. The main arm has a microwave source, an isolator, the first 10 dB directional coupler, a variable attenuator, a three-port circulator, a second 10 dB directional coupler and a Schottky detector. After the first directional coupler come a phase shifter, a 20 dB directional coupler for counting the

Table 1. Technical specifications of three 94 GHz microwave sources.

	Hughes Gunn	Varian Klystron	ZAX Gunn
Model	47276H-1203	VRB2111A-25	ZVT10/50/94.2/0.5
Series #	017	2066C7	241
Freq. bandwidth (GHz)	93.3–94.8 varactor	93.2–94.8 mechanical (±0.2 GHz ETR)	93.95–94.45 varactor
Op. voltage (V)	4.61	2500	10
Op. current (A)	0.752	0.025	0.177
Breakdown voltage (V)	48	—	—
Nominal output power (mW)	35	400	>50
SSB FM noise (dBc/Hz)	−75	−93	−103

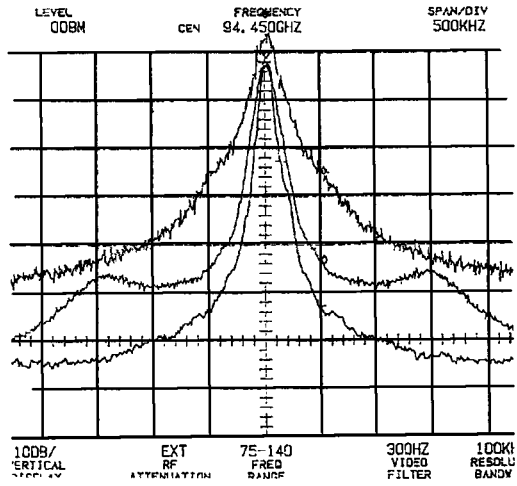

Fig. 2. Comparison of the FM noise among three microwave sources: the Hughes varactor-tuned Gunn oscillator (top), the Varian klystron (middle), the ZAX varactor-tunes Gunn oscillator (bottom).

microwave frequency, and another attenuator for regulating the power throughput of the reference arm; these complete the reference loop. From the second port of the circulator, a vertical arm, consisting of a W-to-Q-band transition (horn), a Q-band oversized waveguide, and a Q- to W-band waveguide transition (the second horn), connects with the resonator.

Attenuation of microwave power at the very high frequency is severe and is exacerbated by the effective doubling of the microwave path between circulator and cavity by the return from the reentrant cavity. In the W-band EPR spectrometer, two measures have been taken to reduce those losses. First, use of oversize (Q-band) waveguide between the circulator and the resonator reduces microwave power loss from 10 to 4 dB/m. Second, the microwave bridge is located below, not above, the Varian magnet, since the vertical center of the superconducting solenoid is closer to the bottom mouth of the magnet than to the top one. The total circulator-to-cavity distance is 38 cm. The entire bridge is mounted on an elevator platform that can be lowered conveniently for sample changing, modification, and adjustment.

Except for the Q-band section and associated transitions, WR-10 waveguide is used throughout the microwave bridge. Appendix A of Wei Wang [14] includes the major suppliers, names, model numbers, and major technical specifications of the W-band microwave components.

Resonator. The heart of the spectrometer is the microwave cavity resonator. This key component was uniquely designed and constructed at IERC. Fig. 3 shows an expanded view of the cylindrical TE_{013} cavity resonator. Table 2 lists key specifications of the resonator.

The cavity itself (part h) is fabricated from machinable ceramic, MACOR (Corning Glass, New York) with a fired-on gold surface heat-deposited from

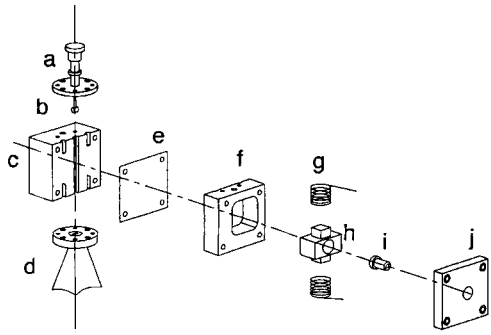

Fig. 3. An exploded view of the TE_{013} cavity resonator. See text for descriptions of the labeled parts.

a metalloorganic gold ink (Engelhard, Specialty Chemicals Division, East Newark, NJ, USA). The cylinder axis (coinciding with the long dot-dash line) is perpendicular to the solenoid axis of the magnet and therefore to the static field. One end of the cavity is terminated by an end plate with a screw tuner (part i), allowing one to vary the length of the cavity in order to adjust its characteristic resonant frequency. A sample access hole is located in the center of the screw tuner.

The other end of the cavity is terminated with a thin metal diaphragm (part e). In the diaphragm is an iris, located one-fourth of a cavity diameter away from the side of the cavity. There are several diaphragm/iris combinations to choose from to allow for a variation of the microwave coupling to the waveguide. The other side of the diaphragm forms a segment of the side wall of the W-band waveguide (the waveguide block, part c). The Q → W transition waveguide (part d) comes from below, passes the cavity, and is terminated by a waveguide stub tuner (part a and part b). To vary the coupling, the stub tuner can be adjusted. This micrometer adjustment, together with the provision for different coupling irises, allows close-to-critical matching of the cavity to the waveguide. The unique block design (parts c, e, f, and j) for the cavity permits the use of a very thin diaphragm (part e,

Table 2. Technical specifications of the EPR cavity resonator.

Cavity mode:	TE_{013}
Center resonance frequency:	94.0 GHz
Frequency tuning range:	±0.5 GHz
Unloaded quality factor Q_u:	4000
Coupling range:	200–2000
Cavity dimension:	$2a = d = 6$ mm; a = length and d = diameter of the cylinder
Cavity volume:	170 µl
Sample size:	0.1–0.8 mm inner diameter and up to 6 mm in length
Sample volume:	16 nl to 3 µl in volume
Maximum filling factor η_{max}:	0.078

ca. 0.10 mm) and at the same time maintains excellent mechanical and thermal stability.

Fused quartz sample tubes (Vitro Dynamics Inc, Rockway, NJ) accommodate typical sample sizes of 0.1 to 0.8 mm inner diameter with a length of 2 to 28 mm. The active sample length is about 2 to 6 mm depending on sample quantity and sample characteristics.

At the 3 mm wavelength, resonator surfaces become much more critical than at the 3 cm X-band wavelength. The fired-on gold surfaces provide a uniform, smooth, and durable metallic layer that is thick enough for obtaining a high quality factor (Q), yet thin enough to let magnetic field modulations penetrate. An important issue is the resistance of these surfaces to cycling between room temperature and cryogen temperatures. A repeated test of dipping the MACOR cavity into liquid nitrogen and then exposing it to air at room temperature has revealed no cracking or visible surface deterioration.

Microwave Detector. Currently, a Hughes tunable single-end mixer or Schottky diode is used, with a preamplifier and bias current supply similar to that in commercial Varian designs [14].

Superconducting Magnet. A Varian XL-200 superconducting NMR magnet (maximum $B_0 = 4.7$ T = 47000 G) together with a locally-constructed room-temperature sweep coil constitute the magnet subsystem, which can accommodate most organic radicals and some of the transition metal ions (g factor range from 1.9801 to 2.0192). This superconducting magnet normally operates in its persistent mode. The long-term stability of the magnet as measured by average field drift over set time periods is much better than 0.05 ppm per hour. The magnetic field run-up is done with a Varian proprietary power supply, normally used for field.

The magnet, as it was constructed for high-resolution NMR, has shim coils which can be used to improve field homogeneity. The field is homogeneous to ±50 milliGauss over a 30 cm^3 space, or ±1.5 ppm over the same space. With a separate air-cooled room temperature sweep coil, the entire spectra of most organic radicals can be observed. To acquire spectra of most transition metal ions, the superconducting magnet must operate in non-persistent mode. Unfortunately, the consumption of liquid helium in this mode is about 350 times higher than in the normal, persistent mode. A straightforward gas-flow cooling accessory (a removable plastic low-temperature jacket connected to a liquid nitrogen heat exchanger, the temperature being regulated by controlling the flow rate of N_2 gas), we have routinely done experiments down to 160 K. The air-cooled sweep coil provides a scan range up to 300 G (0.03 T) at a rate up to 600 $G \cdot s^{-1}$, without affecting the superconducting magnet. The lack of observed interaction is understandable, as the inductances of the sweep coil is quite small.

The disadvantages of this small-bore magnet sub-system are the lack of agility in center field setting, somewhat limited field sweep range, and limited

space to accommodate special accessories and cryostat. Therefore, an alternative large-bore magnet sub-system, which will be described elsewhere, has been set up [15] to circumvent these particular disadvantages. But the advantages of the small-bore system are obvious. They include inherent high field homogeneity and stability, easy maintenance, very low consumption of liquid helium when in persistent mode, and the convenient way the sweep coil operates (very similar to the sweep of a conventional EPR spectrometer system and thus easy to learn and operate).

Electronics and Instrument Control. Gunn oscillator power supply, frequency generator, AFC, preamplifier, magnetic field modulation driver, magnetic field sweep driver (bipolar current amplifier) are all locally built. Schematic drawings are available [14]. The Gunn oscillator power supply, frequency generator, and AFC unit are built into commercially available EG&G ORTEC 4001C BIN modules with ancillary power supply. The SR-530 Lock-in amplifier by Stanford Research System is used to provide the function of phase-sensitive detection and signal amplification. An HP5460A digital oscilloscope is used for tuning the spectrometer and locating the EPR signal by rapid scan. An EIP 578 source-locking microwave frequency counter is used to monitor and track the frequency. In the rare cases where the AFC has difficulty in locking-in, this frequency counter can be used in its Phase Lock Loop (PLL) mode to fix the frequency of the microwave source at the cavity resonant frequency. (This mode is useful only when the cavity resonant frequency stays relatively stable). Precise g values are determined by the ratio of the microwave frequency and the magnetic field strength measured by a high precision field-tracking NMR teslameter by Metrolab (Metrolab PT 2025).

2.3. Performance Tests of the W-band Spectrometer

Sensitivity (or signal-to-noise ratio) is one of the most important performance tests for any general-use EPR spectrometer. A general-purpose spectrometer needs to be able to perform well for a wide range of sample types. Samples are frequently of very limited size or quantity or spin concentration, placing special demands on signal-to-noise ratio. Two kinds of sensitivities are important – point sensitivity, also called absolute sensitivity, measured in terms of minimum detectable number of spins per Gauss ($N_{\min}$); and concentration sensitivity, measured by the minimum detectable concentration ($C_{\min}$) (spins per Gauss per cubic cm). Samples can be classified into at least eight types depending on their degree of dielectric lossiness, ease of saturation, and limitations of sample size. Various sample types will have different microwave-frequency dependence of the sensitivity. Higher microwave frequencies generally are expected to bring much higher sensitivity for a nonlossy, nonsaturating sample of limited size.

For the cylindrical TE_{013} cavity with a Gunn source, we performed sensitivity tests at low power with two samples: the certified NBS (U.S. National Bureau of standards, now NIST, National Institute of standard Technology) ruby specimen with 1 mW power or a 3 μl sample of 5 μM TEMPO in pentane at 2.5 mW. The two measurements are consistent. The TEMPO sample, with 3.6 Gauss peak-to-peak linewidth, was run at 4.0 Gauss modulation amplitude. The low-power result is $N_{min} < 10^9$ spins/G *at 2.5 mW*, better than the conventional X-band and Q-band spectrometer, as expected from the sensitivity-frequency relationship, and comparable with the results from Lebedev's and Möbius' laboratories [1, 5]. On the other hand, because of the much smaller sample size and cavity mode, the concentration sensitivity does not improve, still remaining at $C_{min} \approx 1.3 \cdot 10^{12}$. A previously-published table [2] compares our assessments of sensitivity of our first W-band spectrometer, measured as is customary with nonsaturating low-loss samples, with reports for several other high-field spectrometers. Sensitivity performance of this and other very-high-frequency EPR spectrometers will improve with better technology.

To be widely useful for biological applications, the W-band spectrometer must be able to handle aqueous samples. Samples which cause large dielectric losses at the spectrometer frequency present special problems such as reduced sensitivity. How much reduction is there? Will the reduction be so severe as to render the W-band spectroscopy of a lossy sample impossible? To answer these concerns, we have also measured the W-band spectra of various lossy, especially aqueous, specimens. Fig. 4 shows Q-band spectra of 10 μM TEMPOL in water solution. The signal-to-noise ratio is better than 100 : 1, corresponding to a minimal detectable concentration of 10^{-7} M ($N_{min} \approx 2.4 \cdot 10^{10}$ spins/Gauss). The sensitivity figure of this spectrometer

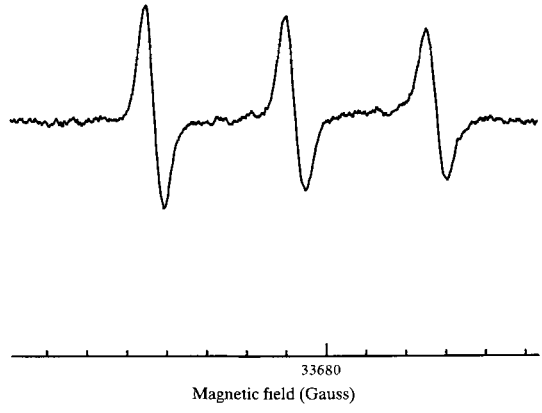

Fig. 4. W-band EPR spectrum of a 10 μM solution of TEMPOL in water. Sample volume is 0.4 μl.

Table 3. Miscellaneous W-band EPR spectrometer performance specifications.

Center frequency:	94.2 GHz, source & cavity tunable
Gunn frequency stability:	0.5 ppm w/PLL; 1.0 ppm w/AFC
Magnetic field stability:	<0.05 ppm/h
Magnetic field sweep linearity:	$r = 0.999$
Center field:	33600 Gauss for $g = 2.0$ sample
Field homogeneity:	± 50 mG for a $r = 2.5$ cm, $h = 1.5$ cm column
Modulation field intensity:	25 Gauss peak-to-peak max.
Modulation frequency:	audio – 2 MHz, normally at 100 kHz
Magnetic field scanning rate:	fast scan, oscillator mode 0.02 to 1 s, slow scan 1 s and up
Temperature control:	160 to >300 K
Magnet servicing interval:	liq. N_2: 10 days, liq. He: 50 days

for an aqueous sample in a small-diameter quartz capillary at W-band is about the same as the sensitivity of a typical Q-band spectrometer.

In order the accurately and reproducibly obtain an EPR spectrum, several other criteria also need to be met. These include the source frequency stability, magnetic field stability, field sweep linearity. The results of the performance tests on these criteria are summarized in Table 3.

3. Benefits of VHF EPR

In previous review articles [1–3], many advantages of performing electron paramagnetic resonance (EPR) experiments outside the traditional 9 to 35 GHz have been clearly stated. Several successful high frequency (>35 GHz) EPR spectrometer systems are reviewed in these articles. The present chapter is intended to illustrate some of the advantages of very high frequency (VHF) EPR with some examples of our own.

One of the most important motivations for doing EPR at very high frequency (VHF) is the potential for better spectral resolution, especially g resolution. By considering the simple resonance condition $h\nu = g\beta H$, one can see easily that the difference in resonant field is proportional to the microwave frequency of the resonance $\Delta H = (h/\beta)\Delta(1/g)\nu$; therefore, it is expected that the resolution of the EPR signal at W-band (95 GHz) will be ten times better than at X-band (9.5 GHz), providing signal linewidths do not increase. Many systems have already demonstrated this enhanced resolution. For instance, Fig. 5 shows the dramatic change in the spectrum of a 100 μM TEMPONE/d-PCA mixture in aqueous solution at room temperature on going from X-band to W-band. At conventional X-band frequency, the difference between the spectral centers of the two nitroxides is smaller than the spectral linewidths. Only three lines appear, as though there were only one nitroxide species. At W-band, the separation of the two spectral centers

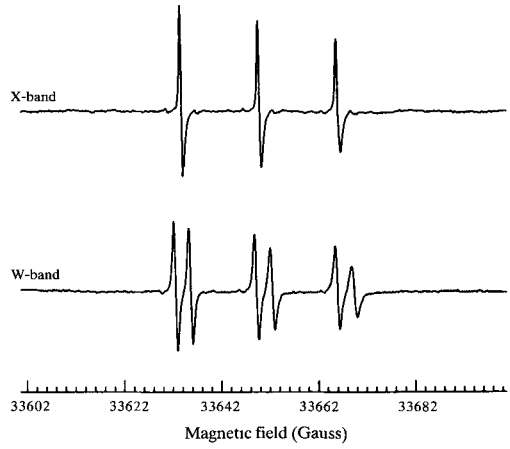

Fig. 5. X-band (top) and W-band (bottom) EPR spectra of TEMPONE/d-PCA (1 : 1) aqueous solution at room temperature. Sample size is 0.1 μl. The magnetic field scale for the W-band spectrum is shown in the plot.

becomes large enough to overcome the spectral linewidths; thus a two-sets-of-three-lines pattern emerges, indicating the co-existence of two different nitroxide species.

Just as different isotropic g factors can be resolved at W-band, so also can anisotropic components of a g tensor in a disordered solid. Fig. 6 illustrates the resolution of principal g tensor components of dibenzothiophene (DBT) cation radicals in boric acid glass at W-band. An EPR g matrix contains information about the molecules being studied. Accurately measuring the g matrix for disordered samples has been difficult, nearly impossible for most

Fig. 6. X-band and W-band EPR spectra of dibenzothiophene (DBT) cation radical, formed by ultraviolet irradiation, in boric acid glass. The magnetic field scan range is 300 Gauss. The X-band spectrum is rescaled from a 100 G scan.

organic radicals which usually only have very small g anisotropy. The ability of very-high-frequency EPR to provide a well defined, single-crystal-like g tensor from a powder spectra of organic radicals in disordered states, as illustrated in Fig. 6, presents an exciting opportunity to study spectral/structure relationships. It also presents the opportunity to using this relationship and VHF EPR spectroscopy to positively identify and characterize various organic and inorganic radicals in synthetic and natural systems.

The second feature of VHF EPR is that by changing the resonance field **B**, it changes the magnitude of field dependent terms relative to field independent terms in the spin Hamiltonian for the system under study:

$$\mathscr{H} = \{\beta \mathbf{B} \cdot \mathbf{g} \cdot \mathbf{S} - \beta_n g_n \mathbf{B} \cdot \mathbf{I}\} + h\mathbf{S} \cdot \mathbf{A} \cdot \mathbf{I} + h\mathbf{I} \cdot \mathbf{P} \cdot \mathbf{I} + h\mathbf{S} \cdot \mathbf{D} \cdot \mathbf{S} + \text{higher order terms}. \quad (1)$$

This change adds a great deal of information to facilitate the interpretation of a spectrum, and often changes the appearance of the spectrum. Especially for powder spectra, the change sometimes produces a simpler spectrum. In such fortunate cases, we can read off relevant EPR parameters directly from the spectrum, as we can do with the g tensor in Fig. 6. In that case, there other example, Fig. 7 shows EPR spectra of a trace amount of Mn^{2+} in soybean flour at three different microwave frequencies. As frequency increases from 9.5 to 35 GHz, and finally to 95 GHz, the effect of second-order contributions from **D** and **E**, decreases with a resultant decrease in the forbidden hyperfine transitions. The spectrum is then simplified, and the hyperfine constant can be read with minimal error directly from the W-band spectrum.

VHF EPR also promises the opportunity to extend the motion sensitivity of the CW EPR to a wider range. For instance, nitroxide molecules need to tumble fast enough in order to completely average out the anisotropies of g and A. For a typical nitroxide DTBN (Di-*tert*-butylnitroxide), the lower limits of the fast tumbling rate (τ^{-1}) are estimated in Table 4. In order that the EPR spectra of nitroxides maintain a sensitivity to motion, their tumbling motion must not completely average out anisotropy due to g and A. The lower limit of the tumbling rate is the so-called fast tumbling limit, where $\tau^{-1} \gg \Delta\omega_{an}$. Unless the tumbling rate is large enough to average out the anisotropy, the observed spectrum will not be characteristic of the fast motion regime. Note that W-band exerts a ten-times-higher apparent tumbling rate for fast motion. This shows that at W-band, spectral sensitivity to faster motion will be possible. This also implies that since the molecules tumble at certain rate at a given temperature, fast-motion spectra observed at 9.5 GHz may not be fast enough to be averaged at 95 GHz and slow-motion spectra of lower frequency can even approach to the rigid limit at higher frequency. Thus, in some cases, one might hope to observe a powder-

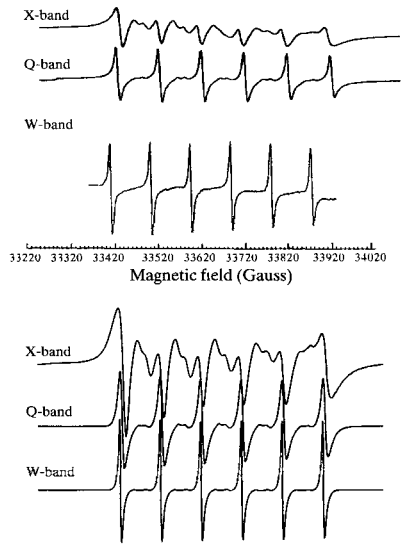

Fig. 7. EPR spectra ($|+1/2\rangle \longleftrightarrow |-1/2\rangle$ transition) of a trace amount of Mn^{2+} in soybean flour at three different microwave frequencies: 9.5, 35 and 95 GHz. Top three: the experimental; bottom three: the simulated.

like spectrum and extract the rigid-limit magnetic parameters without completely immobilizing the sample. This could be useful for studying the structure and dynamics of membrane bound biological radicals or metalloproteins.

Finally, with the higher intrinsic transition intensity (due to a greater population difference in spin states) and shorter wavelength of microwaves at W-band, we can work with much smaller samples. Table 5 shows the product of filling factor η (assuming constant sample size) and typical values of quality factor Q for a TE_{011} cavity at X-, Q- and W-band.

We see immediately from the table that the product of η and Q increases more than two orders of magnitude from the X-band to W-band. Since the signal intensity of an EPR absorption is proportional to $\eta Q P_0$, we expect better sensitivity for size limited samples at the higher frequency. This is indeed what we have observed in many applications of VHF EPR. For example, neuromelanin from human *substantia nigra* is very difficult to prepare (only 0.1 mg per subject), very often a fraction of *ca.* 1 mg sample is all one can get. So this is a typical size-limited sample and signal-to-noise

Table 4. Lower limit of the fast tumbling rate of DTBN.

	X-band, 9.5 GHz (rad · s^{-1})	W-band, 95 GHz (rad · s^{-1})
$\Delta\omega$ due to g_{an}	$0.18 \cdot 10^{-9}$	$1.80 \cdot 10^{-9}$
$\Delta\omega$ due to A_{an}	$0.45 \cdot 10^{-9}$	$0.45 \cdot 10^{-9}$

Table 5. Comparison of TE_{011} cavities at various microwave frequencies.

	X-band[1]	Q-band[1]	W-band[2]	D-band[3]
Frequency (GHz)	10	35	100	150
Cavity size d (cm)	4.00	1.14	0.40	0.27
Cavity volume V_c (ml)	50.24	1.16	$5.02 \cdot 10^{-2}$	$1.72 \cdot 10^{-2}$
Sample size i.d. $\times l$ (mm)	0.8×6	0.8×6	0.8×6	0.7×2.7
Sample volume V_s (ml)	$3.01 \cdot 10^{-3}$	$3.01 \cdot 10^{-3}$	$3.01 \cdot 10^{-3}$	$1.04 \cdot 10^{-3}$
Filling factor η	$6.0 \cdot 10^{-5}$	$2.6 \cdot 10^{-3}$	$6.0 \cdot 10^{-2}$	$6.0 \cdot 10^{-2}$
Unloaded Q_u	20000	10000	3150	2000
ηQ_u	1.2	26	189	120

[1] From Varian EPR manuals (Varian Associate, Palo Alto, CA).
[2] Measurements of the TE_{013} and extrapolating to TE_{011}.
[3] From Grinberg *et al.* [1].

ratio (S/N) is much better at W-band. Another prospective utilization of the increased sensitivity is the study of metalloproteins, where most proteins are hard to crystallize, and even when they can be successfully crystallized, they are usually very small.

We have just touched an important issue in any spectroscopy, namely, sensitivity. Sensitivity in EPR spectroscopy is dependent on resonance frequency, partly due to the greater population difference of spins at higher magnetic field. Theoretically, the sensitivity increases, or the minimum detectable number of spins decreases, as ω^x [16], where x varies from 1/2 to 9/2 and is dependent on whether or not 1) the sample is size limited; 2) the sample can be saturated; or 3) the sample has negligible dielectric loss [17]. Practically, however, the "engineering factors" (e.g. the noise figure F of the spectrometer system, or quality factor Q_u of the cavity resonator) play important roles in determining the S/N performance of a spectrometer system.

4. VHF EPR as an Integral Part of a Multifrequency Strategy: An Example

The resolution of an EPR spectrum depends on the spectral linewidth. However, there is little literature dealing with electron spin relaxation and other linewidth-broadening mechanisms in the context of a widely varied EPR resonance frequency. But knowing the frequency dependences of EPR linewidths can certainly help us to design our experiments more efficiently, and such data also contain certain information on the system being studied. Therefore, we are accumulating experimental data on particular systems at different microwave frequencies and are trying systematically to examine the frequency dependences of predicted EPR spectra.

We have observed that the EPR linewidths of many organic radicals do not broaden substantially from 9.5 to 95 GHz, so the high resolution condition holds for these systems. A condition for high g resolution in solid state EPR can be expressed most simply as:

$$|g_x - g_y| h\nu/\beta g^2 > (\Delta H_{0x} + \Delta H_{0y} + |A_x| + |A_y| + |\delta g_x| + |\delta g_y| + |\delta A_x| + |\delta A_y|),$$

$$|g_y - g_z| h\nu/\beta g^2 > (\Delta H_{0y} + \Delta H_{0z} + |A_y| + |A_z| + |\delta g_y| + |\delta g_z| + |\delta A_y| + |\delta A_z|), \quad (2)$$

where $\Delta H_{0x,0y,0z}$ are intrinsic linewidths (T_1 and T_2 broadening) and $g_{x,y,z}$, $\delta g_{x,y,z}$ and $A_{x,y,z}$, $\delta A_{x,y,z}$ are principal g and hyperfine coupling values and their variance (strain), respectively.

One also should ask the questions: "how high a frequency is high enough?" Or "is higher always better?" Undoubtedly there are some questions about certain systems that require a very high frequency to answer; however, such extremely high field or high frequency can also impose severe technical limitations. So far, the highest field reported is 100 T, realized by a pulsed magnet [18], but due to the obligatory broad recording bandwidth (for a 200 μs pulse duration, a 10 G signal corresponding to 2 ns, a bandwidth of 500 MHz) and the very low duty cycle, the concentration sensitivity was rather low. Besides, it is almost impossible to avoid a large distortion of the signal, which cannot be easily analyzed.

Therefore, as a general methodology, it might be better to work at several frequencies than to work at just one extremely high frequency. Elements of spin Hamiltonian parameters in Eq.(1), **g**, **A**, **P** and **D**, that have been determined by a multifrequency strategy are subject to much less uncertainty than a single-frequency determination [2, 3]. Consider a Cu(II) ($S = 1/2$, $I = 3/2$) square planar site, for example, at X-, Q-, W-, D-, and G-band in Fig. 8 (Case A). This is a set of simulations of a system similar to copper (II) bisdiethyldithiocarbamate [19]. The principal values of g and A tensors are $g_{x,y,z} = (2.0166, 2.0246, 2.0856)$ and $A_{x,y,z} = (103.5, 115.5, 468.5)$ MHz. The linewidth is set proportional to microwave frequency to emulate the g-strain broadening $B(\delta g)$; the linewidth at Q-band is set to be 17.50 MHz. To address one aspect of the skepticism about the usefulness of high frequency EPR, we intend to show that the loss of resolution of **A** or **P** will not render VHF EPR useless. In the Fig. 8, we see 1) a sharp X-band spectrum but $g_{x,y,z}$ components all mixed together; 2) a partly resolved Q-band spectrum but with perpendicular x and y hyperfine components interpenetrating; 3) a rather easily interpretable W-band spectrum with g_x and g_y region nearly resolved, each with clear hyperfine structure; 4) a D-band (140 GHz) spectrum in which the hyperfine structure at perpendicular region is almost obscured by the g-strain broadening (the rhom-

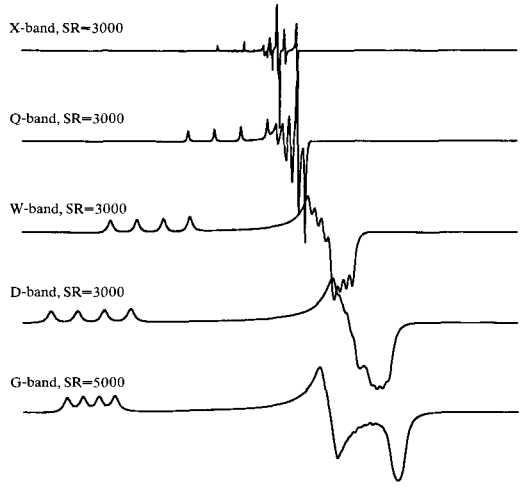

Fig. 8. Simulated EPR spectra of Cu(II) square planar site similar to Cu(II) bisdiethyldithiocarbamate at 9.5, 35, 95, 150 and 250 GHz. See text for the simulation parameters, Case A.

bic g anisotropy is not quite revealed in the envelope of the perpendicular region); and 5) a G-band (250 GHz) spectrum clearly showing the classic shape for a rhombic spectrum with no perpendicular hyperfine structure. From the G-band spectrum, one can directly measure the canonical components of the g tensor (principal g values). In the second series (Fig. 9), we see a case (Case B) in which the rhombic g anisotropy is doubled (2.0126, 2.0286, 2.0856) but the linewidth is tripled (Q-band linewidth 52.5 MHz,

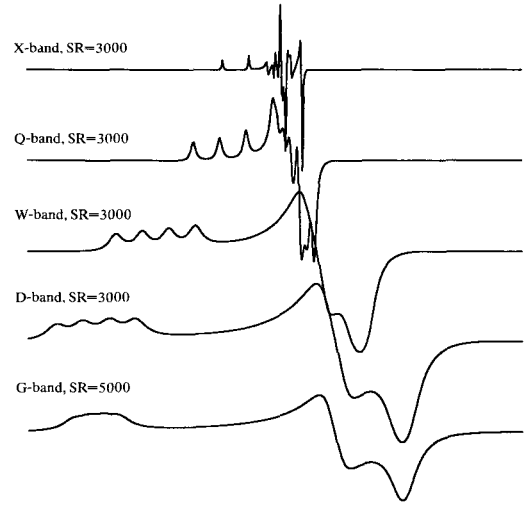

Fig. 9. Simulated EPR spectra of Cu(II) square planar site similar to Cu(II) bisdiethyldithiocarbamate at 9.5, 35, 95, 150 and 250 GHz. See text for the simulation parameters, Case B.

linewidth is set proportional to frequency). Here, all the hyperfine resolution is lost between W- and G-bands, but all three VHF bands show clear rhombic resolution. In all cases, the most reliable interpretations will be obtained from a multi-frequency approach.

By examining the EPR parameters as functions of frequency, we can get a so-called frequency dispersion profile of the EPR parameters. The individual spectrum at each frequencies is interesting by itself, and adds valuable structural or dynamic information about the system being studied. Apparently, the use of only one or two frequencies cannot yield such a profile. We need at least three to start to see any trend; of course, four or five will be even better.

Now we consider the final example – the primary electron donor P_{865}^{+} in photosynthetic bacterial reaction centers of *Rhodobacter sphaeroides* R-26. Reaction centers (RC) are membrane bound, proteinaceous complexes where a variety of chemical and photochemical reactions take place in the photosynthetic bacteria to produce a proton gradient. P_{865}^{+} is a double-decker – a so-called "special pair" of *Bacteriochlorophyll a* molecules embedded in the RC from *Rhodobacter Sphaeroides* R-26. It functions as the primary electron donor. Owing to its central role in photosynthesis, considerable interest has been attracted to the study of structure and function of the special pair. EPR has been quite successful in revealing the structure of the P_{865}^{+} cation radical. For example, Norris *et al.* [20] showed, first with EPR and then with ENDOR, that the primary donor in reaction centers of R-26 is a special pair of bacteriochlorophyll molecules. But due to the immobilization of the radical and the large number of nuclei interacting with the electron, conventional EPR at X- or Q-band produces only a single, broad, featureless, and fairly uninformative spectrum.

The EPR g tensor, if measurable, can play a role in characterizing and understanding the reaction center. Although only slightly explored to date, g anisotropy has the potential of helping us to understand the electronic structure of the special-pair radical ion produced by the primary photosynthetic event. In addition, precise measurement of the g matrix is an important adjunct to ENDOR, ESE, and spin polarization studies.

In addition to the normally grown specimens, fully deuterated *Rhodobacter Sphaeroides* R-26, grown in a medium containing 99.7% D_2O solution of deuterated succinic acid as a source of carbon and deuterated algae hydrolyzate, was prepared in Argonne National laboratory. Reaction centers are isolated from both protonated and deuterated R-26. The cation species P_{865}^{+} is produced by oxidizing reaction centers with $K_3Fe(CN)_6$ in water and deuterated water, respectively. Both the protonated and deuterated specimens are prepared for spectral examination with both H_2O and D_2O. This cross-check reveals no effect on the spectra, which in turn suggests that the linewidth is not affected by exchangeable protons.

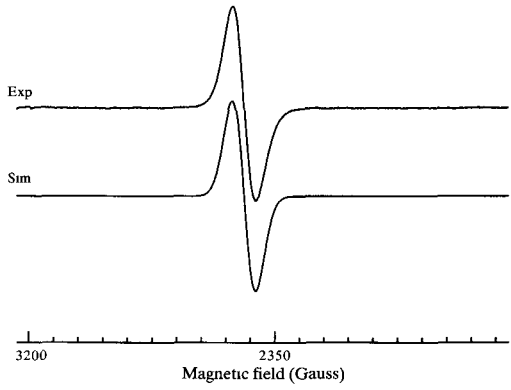

Fig. 10. Experimental and simulated EPR spectra of deuterated P_{865}^{+} at X-band. The simulation uses the g matrix obtained from W-band and best-fit linewidth for X-band.

W- and X-band EPR spectra of the primary electron donor P_{865}^{+} in both protonated and deuterated photosynthetic bacterial reaction centers of R-26 are shown in Figs. 10 to 13. (Q-band spectra also have been obtained and are consistent with our analyses [14]). We see immediately that isotope substitution of ^{1}H with ^{2}H narrows the linewidth across all frequencies (therefore unresolved proton hyperfine structure contribute to the linewidth) and as a result, the W-band spectrum of deuterated P_{865}^{+} is resolved. Computer-assisted spectral simulation and analysis are carried out to extract principal g values form the spectrum. They are, in an arbitrarily decreasing order,

$$g_a = 2.00334\,, \quad g_b = 2.00246\,, \quad g_c = 2.00221\,; \quad \langle g \rangle = 2.00267\,.$$

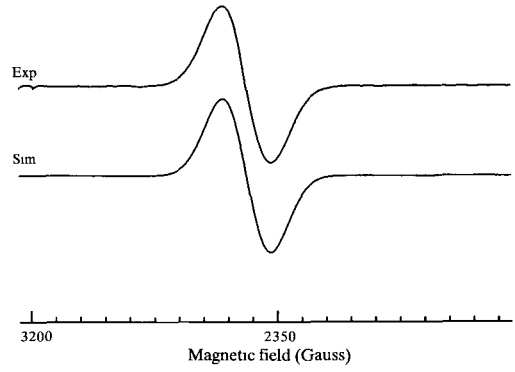

Fig. 11. Experimental and simulated EPR spectra of protonated P_{865}^{+} at X-band. The simulation uses the g matrix obtained from W-band and best-fit linewidth for X-band.

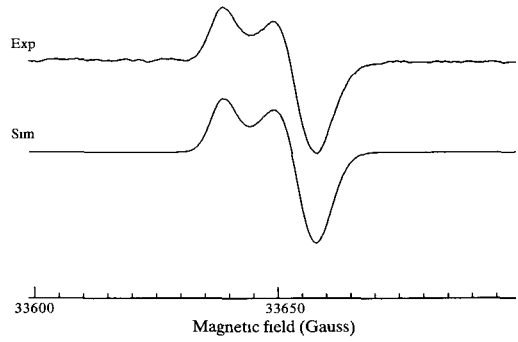

Fig. 12. Experimental and simulated EPR spectra of deuterated P_{865}^{+} at W-band. The simulation provides the best-fit g matrix and linewidth. The g matrix is then used to simulate every other spectrum.

These values are in reasonable accord with Burghaus *et al.* [21], who obtained and analyzed W-band spectra of protonated P_{865}^{+} reaction centers from R-26. P_{865}^{+} is thought to be a pair of bacteriochlorophylls (dimeric cation radical form), presumable resembling a delocalized π-radical. The averaged g factor does not refute this point of view, as $\langle g \rangle = 2.00267$ is a typical value for a carbon based π-radical. Interestingly, the apparent rhombic g factors can be grouped either by forcing $g_{\perp} = (g_a + g_b)/2$, $g_{\parallel} = g_c$ [22] or $g_{\perp} = (g_b + g_c)/2$, $g_{\parallel} = g_a$. Both groupings can give similar fits at Q-band or lower frequency, but the latter seem to be more reasonable as judged by the g tensor and EPR lineshape measured at W-band.

These principal g values are then hold constant and variable linewidths are used for best fits to all other spectra. All the spectra have been simulated

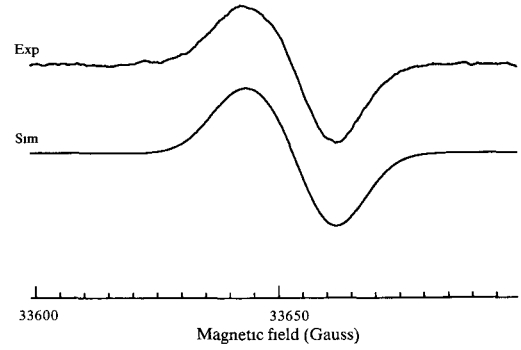

Fig. 13. Experimental and simulated EPR spectra of protonated P_{865}^{+} at W-band. The simulation uses the g matrix obtained from W-band for the deuterated counterpart and best-fit linewidths for this spectrum.

with Gaussian lineshapes, as is consistent with the notion that the EPR signal of R-26 is inhomogeneously broadened. We have carried out a multifrequency linewidth analysis (see Wang [14] for details; to be published) along the lines of McElroy *et al.* [23]. The frequency dependences of the principal linewidth components of native and deuterated P^+_{865} are quite consistent with a model including g-strain with significant contributions from unresolved nitrogen and nonexchangeable proton or deuteron hyperfine structure. The linewidth behavior suggests that the radical is part of a rigid structure with minimum motional effect, consistent with our experimental observation that changing the temperature from -110 to -60°C has no effect on the apparent linewidths. From the frequency dependences of the linewidths and from the g matrix, we can predict spectra at other frequencies; preliminary results at 140 GHz [24] for the native P^+_{865} are consistent with our extrapolation.

Finally, it is interesting to compare the g matrix reported here for P^+_{865} with that reported by Prisner *et al.* [25] for the $P700^{+0}$ center from deuterated cyanobacterial PS-I particles, as measured from 140 and 9.5 GHz EPR:

$$P^+_{865} : 2.00221,\ 2.00246,\ 2.00334,$$
$$P700^{+0} : 2.00232,\ 2.00262,\ 2.00304.$$

There are clearly differences. First, the g anisotropy appears considerably larger in the P^+_{865} center. Second, although the lowest g component of each center is close to the free-electron value, it is slightly lower than g_e for P^+_{865} but higher than g_e for $P700^{+0}$. It would be interesting to examine the possible electronic and molecular structural implications of these differences, but that is beyond the scope of this report.

Acknowledgements

We acknowledge useful conversations with Drs. K. Möbius, G. Gerfen, R. G. Griffin, Ya. S. Lebedev, J. Freed, F. P. Auteri, P. Kovacz, K. Ho, and A. I. Smirnov. Support was derived from the U.S. Department of Energy, the University of Illinois Research Board, the National Institutes of Health (RR01811 and GM42208), and the Illinois Department of Energy through its Coal Development Board and Illinois Clean Coal Institute. However, opinions, findings, conclusions, and recommendations are those of the authors and do not necessarily reflect the views of the sponsoring agencies.

References

[1] Grinberg O.Ya., Dubinskii A.A., Lebedev Ya.S.: Russian Chemical Reviews **52**, 850 (1983)

[2] Belford R.L., Clarkson R.B. in: Magnetic Resonance of Carbonaceous Solids (Botto R.E., Sanada Y., eds.). ACS Advances in Chemistry Series **229**, 107–138. Washington DC: ACS 1993.

[3] Belford R.L., Clarkson R.B., Cornelius J.B., Rothenberger K.S., Nilges M.J., Timken M.D in: Electron Magnetic Resonance of the Solid State, (Weil J.A., ed.). CSC Symposium Series Vol.1, 21. Ottawa: Canadian Society for Chemistry 1987.

[4] Barra A.L., Brunel L.C., Robert J.B.: Chem. Phys. Lett. **165**, 107 (1990)

[5] Haindl E., Möbius K., Oloff H.: Z. Naturforsch. **40a**, 169 (1985)

[6] Box H.C., Freund H.G., Lilga K.T., Budzinski E.E.: J. Phys. Chem. **74**, 40 (1970)

[7] Budil D.E., Earle K.A., Lynch W.B., Freed J.H. in: Advanced EPR in Biology and Biochemistry (Hoff A.J., ed.). Amsterdam: Elsevier 1989.

[8] Lynch W.B., Earle K.A., Freed J.H.: Rev. Sci. Instrum. **59**, 1345 (1988)

[9] Wagner R.J., White A.M.: Solid State Commun. **32**, 399 (1979)

[10] Wang W., Clarkson R.B., Auteri F.P., Kovacs P, Williamson M.V., Belford R.L.: Am. Chem. Soc. Preprints, Div. Fuel Chem. **37**, 1141–1150 (1992)

[11] Weber R.T., Disselhorst J.A.J.M., Prevo L.J., Schmidt J., Wenckebach W.Th.: J. Magn. Reson. **81**, 129 (1989)

[12] Clarkson R.B., Wang W., Brown D.R., Crookham H.C., Belford R.L.: Fuel **69**, 1405 (1990)

[13] Clarkson R.B., Wang W., Brown D.R., Crookham H.C., Belford R.L. in: Magnetic Resonance of Carbonaceous Solids (Botto R.E., Sanada Y., eds.). ACS Advances in Chemistry Series **229**, 507–528. Washington DC: ACS 1993.

[14] Wang W.: Very High Frequency EPR: Instrument and Applications, Ph.D. Thesis, University of Illinois, Urbana-Champaign, IL, USA, April 1993 (Copies available through Dissertation abstracts, Ann Arbor, MI, USA)

[15] Nilges M.J., Smirnov A.I., Belford R.L., Wei W., Clarkson R.B.: W-band (94 GHz) EPR System with Fast Sweep and Cryostat. 16th Intl. EPR Symposium at 35th Rocky Mountain Conference on Analytical Chemistry, Denver, CO, USA. July 27, 1993.

[16] Poole Jr. C. P.: Electron Spin Resonance. A Comprehensive Treatise on Experimental Techniques. 2nd edition. New York: Wiley-Interscience 1983.

[17] Wertz J. E., Bolton J. R.: Electron Spin Resonance. Elementary Theory and Practical Applications. New York: McGrow-Hill 1972.

[18] Kuroda S., Motokawa M., Date M.: J. Phys. Soc. Japan **44**, 1797 (1978)

[19] White L.K.: Ph. D. Thesis, University of Illinois, Urbana-Champaign, IL (1975)

[20] Norris J.R., Uphaus R.A., Crespi H.L., Katz J.J.: Proc. Natl. Acad. Sci. **68**, 625 (1971)

[21] Burghaus O., Plato M., Bumann D., Neumann B., Lubitz W., Möbius K.: Chem. Phys. Lett. **185**, 381 (1991)

[22] Allen J.P., Feher G.: Proc. Natl. Acad. Sci. Us. **81**, 4795 (1984)

[23] McElroy J.D., Feher G., Mauzarall D.C.: Biochim. Biophys. Acta **267**, 363–374 (1972)

[24] Gerfen G., Griffin R.G.: MIT, private communication.

[25] Prisner T.F., McDermott A.E., Un S., Norris J.R., Thurnauer M.C., Griffin R.G.: Proc. Nat. Acad. Sci. USA, accepted for publication.

Author's address: Prof. Dr. R. L. Belford, Illinois EPR Research Center, Departments of Chemistry, Internal Medicine and Veterinary Clinical Medicine, University of Illinois at Urbana/Champaign, 506 S. Mathews, Urbana, Illinois, 61801, USA